Tellus
SERIES A
DYNAMIC
METEOROLOGY
AND OCEANOGRAPHY
PUBLISHED BY THE INTERNATIONAL METEOROLOGICAL INSTITUTE IN STOCKHOLM

Tellus (2011), 63A, 893–906
Printed in Singapore. All rights reserved

TELLUS

Impact of increasing resolution and a warmer climate on extreme weather from Northern Hemisphere extratropical cyclones

By ADRIAN J. CHAMPION*, KEVIN I. HODGES[1], LENNART O. BENGTSSON[1], NOEL S. KEENLYSIDE[2] AND MONIKA ESCH[3], [1]*National Centre for Earth Observation, University of Reading, Reading, UK;* [2]*Leibniz Institute of Marine Sciences, IFM-GEOMAR, West Shore Campus, Duesternbrooker Weg 20,* D-24105 *Kiel, Germany;* [3]*Max Planck Institut fr Meteorologie, Bundesstr.* 53, 20146 *Hamburg, Germany*

(Manuscript received 5 April 2011; in final form 5 July 2011)

ABSTRACT

The effect of a warmer climate on the properties of extratropical cyclones is investigated using simulations of the ECHAM5 global climate model at resolutions of T213 (60 km) and T319 (40 km). Two periods representative of the end of the 20th and 21st centuries are investigated using the IPCC A1B scenario. The focus of the paper is on precipitation for the NH summer and winter seasons, however results from vorticity and winds are also presented. Similar number of events are identified at both resolutions. There are, however, a greater number of extreme precipitation events in the higher resolution run. The difference between maximum intensity distributions is shown to be statistically significant using a Kolmogorov–Smirnov test. A generalized Pareto distribution is used to analyse changes in extreme precipitation and wind events. In both resolutions, there is an increase in the number of extreme precipitation events in a warmer climate for all seasons, together with a reduction in return period. This is not associated with any increased vertical velocity, or with any increase in wind intensity in the winter and spring. However, there is an increase in wind extremes in the summer and autumn associated with tropical cyclones migrating into the extratropics.

1. Introduction

In recent years, the damage and disruption that can be caused by extratropical cyclones has been experienced by western Europe, as well as many other places around the world. This damage has resulted from the strong winds, extreme precipitation or a combination of the two associated with extratropical cyclones. For example, during the summer of 2007, the United Kingdom experienced three separate extreme rainfall events that were each associated with an extratropical storm (Blackburn et al., 2008). These events led to extensive flooding in both northern and southern England, affecting hundreds of thousands of people (Pitt, 2008). In Germany, there were 100 fatalities, as well as nine billion Euros of damage, when the River Elbe flooded during August 2002 (Ulbrich et al., 2003) due to extreme rainfall over western and central Europe. During November 2009, Cumbria (United Kingdom) experienced extensive flooding, resulting in 1500 properties being flooded and a death, due to extreme rainfall associated with an extratropical storm (Sibley, 2010). In October 2010, a large part of the United States was affected by floods due to extreme rainfall from an extratropical storm (Grumm, 2010). In December 1999, windstorm 'Lothar' caused billions of Euros in damage and over 50 deaths due to extreme winds (Wernli et al., 2002). These types of storm events can occur at any time of year, though 'windstorms' tend to be more prevalent in the winter period when baroclinic processes dominate and very intense precipitation is often more prevalent in the summer period when convective processes are more important. The risk from extreme winds and precipitation associated with extratropical storms and possible increases in the future, both during winter and summer, poses a serious threat to many mid-latitude regions including the United Kingdom and western Europe. This includes tropical cyclones undergoing extratropical transition. The aim of this study is to investigate the effect of both model resolution and a warmer climate on wind and precipitation extremes associated with extratropical storms, with a particular focus on the precipitation during winter (DJF) and summer (JJA) periods.

The response of the hydrological cycle to a warming climate depends on the robustness of the response to the increase in temperature, Held and Soden (2006) discuss that there is confidence that lower tropospheric water vapour will increase as the

*Corresponding author.
e-mail: a.j.champion@reading.ac.uk
DOI: 10.1111/j.1600-0870.2011.00538.x

climate warms. Although the Clausius–Clapeyron equation predicts a 7% per Kelvin increase in water vapour, it is important to note that global mean precipitation does not increase as rapidly. One consequence of the increase in lower tropospheric water vapour is an increase in the horizontal water vapour transport within the atmosphere, causing an enhancement of the precipitation minus evaporation (P−E), that is, wet areas get wetter and dry areas get drier. Therefore, assuming the lower tropospheric relative humidity is unchanged and that the flow is unchanged, the poleward vapour transport, and the P−E increases proportionally to the lower tropospheric water vapour (Held and Soden, 2006). Therefore, we can expect an increase in the precipitation from extratropical storms in a warmer climate. This is supported by several studies that also suggest that a shift toward heavier intense precipitation can be expected over large parts of Europe in a warming climate (Frei et al., 1998), in particular, the summer period (Christensen and Christensen, 2004).

The focus of this study is synoptic-scale extratropical storms with typical lifetimes of several days and travelling thousands of kilometres. Increases in computational power have meant that global climate models (GCMs) can be run at much higher resolutions, with the ECHAM5 GCM used in this study being run at a T319 resolution, which equates to a 40-km horizontal resolution in comparison to the similar earlier Bengtsson et al. (2009) study which used the same model run at T213 which equates to a 60-km resolution. The study of Bengtsson et al. (2009) has shown that the ECHAM5 model is capable of simulating extratropical cyclones with great realism.

The previous study of Bengtsson et al. (2009) showed that significant increases in the cumulative precipitation along the cyclone tracks are expected in a warmer climate, up to twice the increase in global precipitation. It was also shown that extreme precipitation was found to increase close to the globally averaged increase in column water vapour, around 27% (Bengtsson et al., 2009). In this study, we will explore the impact of resolution on these results.

Other studies have used regional climate models (RCMs) to investigate the effect of a warmer climate on precipitation for a localized area (Fowler et al., 2007; Maraun et al., 2010; Nikulin et al., 2011). RCMs typically have greater resolutions than GCMs, with resolutions typically of the order of 50 km, suggesting they are capable of representing the spatial patterns in extreme precipitation events that are not resolved by GCMs (Fowler et al., 2007). However, these patterns may be dependent on the driving model boundary conditions. RCM studies by Nikulin et al. (2011), using an RCM with a resolution of 49 km, suggest that the recurrence time of intense precipitation reduces in a warmer climate over northern and central Europe, that is, precipitation extremes will become more frequent in both summer and winter. The conclusions from the investigation in this paper using a high-resolution GCM at resolutions comparable to the RCM studies will be briefly compared to the conclusions from these RCM studies.

The paper continues in Section 2 with a description of the GCM simulation, how storms are identified in the model and the method for retrieving the properties of the tracked storms. Section 3 discusses the effect of the higher resolution on the properties of the storms and also looks into the effect of a warming climate on these events. Section 4 discusses the results and gives conclusions.

2. Experiment setup and analysis methodologies

This study uses the Max-Planck Institute (MPI) ECHAM5 atmosphere model (Roeckner et al., 2003) integrated at a T319 spectral resolution (ca. 40 km) with 31 levels in the vertical using the 'time-slice' method. The climate is simulated for two 20-yr periods that are representative of the end of the 20th (1980–2000) and 21st (2080–2100) centuries, using the IPCC scenario A1B (Nakicenovic et al., 2000). These will be hereafter referred to as 20C and 21C, respectively. This is a higher resolution integration than the one used by Bengtsson et al. (2009), which used a T213 spectral resolution (ca. 60 km) of the same model. In the T213 run, the integration was run for 30 yr in each climate (1960–1990 and 2070–2100) rather than 20 yr in the T319 run. The boundary forcings, the SST and sea ice fraction data, are from ensemble member 2 of the T63 (ca. 208 km) ECHAM5 coupled model integrations for the A1B scenario produced for the IPCC AR4 (Roeckner et al., 2006). The SST and sea fraction data are interpolated from the original T63 resolution to the T319 resolution. Both simulations have also previously been used to study tropical cyclones (Bengtsson et al., 2007).

Cyclones are identified and tracked using the TRACK software developed by Hodges (1995, 1999) which here uses the 850-hPa relative vorticity field (ξ_{850}) to identify and track the storms. The vorticity field was chosen as it is less influenced by the large-scale background flow than mean sea level pressure (MSLP). It also focuses on smaller spatial scales and allows systems to be identified much earlier in their lifecycle (Hoskins and Hodges, 2002). The tracking is performed at a reduced resolution of T42 to enable reliable tracking of the storms as high-resolution vorticity data can be very noisy (Hoskins and Hodges, 2002, for details) however, this still identifies more cyclones than is typically the case when using higher resolution MSLP fields (Froude, 2010). Posttracking filters are applied to consider only those storms that last more than 2 d and travel further than 1000 km although we test the sensitivity of the results to these settings. Extratropical storms for both hemispheres and all seasons have been investigated, however the Northern Hemisphere (NH) is the main focus in this paper. Storms that originate in the tropics but move into the extratropics are included, however, tropical storms that have their entire lifecycle in the tropics are excluded. The properties of the storms, such as vorticity, wind speed and precipitation, are determined along the tracks at the full T319 resolution, similar to that performed in the T213 simulation by Bengtsson et al. (2009).

The full resolution properties of storms are added back onto the vorticity tracks using a search within a 5° spherical arc radius from the storms centre for each field. This was found to be sufficient to capture the extremes. Precipitation is computed as the area average within this radius. The vertical velocity is also calculated as the area average within the 5° area. The 850-hPa maximum winds were obtained as a direct search for the maximum within the region as is the maximum vorticity at full resolution. The 850-hPa winds were used as these were the only low-level winds available in the T319 run rather than the 925-hPa winds used by Bengtsson et al. (2009). The 850-hPa winds from the T213 run are also used for comparison in this study.

Intensity distributions of maximum winds and vorticity, minimum area averaged vertical velocity (ascent) and precipitation along the tracks are calculated. Two statistical analyses were performed on these distributions for all the seasons for both resolutions. A Kolmogorov–Smirnov (KS) two-sample test was performed to determine whether the increase in resolution causes a statistically significant change in the distributions under the null hypothesis that they belong to the same underlying distribution (Table 1), this compares the whole of the distributions. The KS test is a non-parametric test. Parametric tests, which typically have a stronger statistical power than non-parametric tests, are difficult to use on these distributions as there is no guarantee that the distributions satisfy the assumptions for a parametric test. The statistical power of a test is the probability of falsely rejecting the null hypothesis, increasing power reduces the chance of a false rejection. Other non-parametric tests, such as the Mann–Whitney U-test, were investigated however it was decided that the KS two-sample test was most appropriate for investigating changes in the shapes of the distributions. The KS test involves creating a cumulative frequency distribution for each resolution, variable, climate and season, using the same bin size for all. These are subtracted from each other at each interval, with the focus being on the largest of these deviations. Two distributions drawn from the same population would be expected to be fairly similar except for random deviations from the population distribution. If the two distributions are 'too far apart' at any point then this suggests that the two distributions come from different population distributions (Siegel, 1956). A p-value of less than 0.05 (95%) is chosen as the level at which the null hypothesis should be rejected.

The second of the statistical analyses was to evaluate the tails of the distributions using extreme value theory (EVT) statistics. In this paper, a threshold model, the generalized Pareto distribution (GPD), is used, where all events that exceed a high threshold are considered as extreme, that is, the tails of the distributions. This is known as a peaks-over-threshold (POT) approach. The generalized extreme value (GEV) distribution, a block maxima approach, was considered but not used since if one block contains more extremes than another, the GEV method can be wasteful of data (Coles, 2001), as is the case in this study. The resulting POT distributions are approximately described by the GPD.

$$H(y) = 1 - \left(1 + \frac{\psi y}{\tilde{\sigma}}\right)^{-1/\psi}, \tag{1}$$

Table 1. Results of the Kolmogorov–Smirnov two-sample test, evaluating whether the increase in resolution is showing a statistically significant change in the distributions, for every field and climate

Variable	Climate		DJF	JJA	SON	MAM
Winds	20C	D	0.0167	0.0279	0.0184	0.0139
		p	0.1244	**0.0026**	0.0883	0.2962
	21C	D	0.0223	0.0354	0.0224	0.0114
		p	**0.0178**	**0.0000**	**0.0244**	0.5719
Vorticity	20C	D	0.0904	0.119	0.1116	0.0901
		p	**0.0000**	**0.0000**	**0.0000**	**0.0000**
	21C	D	0.0925	0.1368	0.1117	0.0965
		p	**0.0000**	**0.0000**	**0.0000**	**0.0000**
Vertical velocity	20C	D	0.4948	0.4439	0.9108	0.916
		p	**0.0000**	**0.0000**	**0.0000**	**0.0000**
	21C	D	0.506	0.4683	0.9186	0.9098
		p	**0.0000**	**0.0000**	**0.0000**	**0.0000**
Precipitation	20C	D	0.0267	0.0398	0.0254	0.0246
		p	**0.0003**	**0.0000**	**0.0054**	**0.0051**
	21C	D	0.0397	0.0285	0.0267	0.012
		p	**0.0000**	**0.0023**	**0.0037**	0.4991

Notes: The D row is the maximum separation observed between the two distributions, the p row is the p-value. The p-value is the probability that a more extreme value can be achieved. A p-value of less than 0.05 (95%) is chosen as the level at which the null hypothesis should be rejected, being marked in bold. Any value that was $<1 \times 10^{-4}$ is shown to have a value of 0.0000.

where

$$\tilde{\sigma} = \sigma + \psi(u - \mu), \tag{2}$$

y is the distribution being analysed, ψ is the shape parameter, σ is the scale parameter, which is a measure of the spread of the distribution and μ is the location parameter. The GPD theorem implies that the threshold excesses have a corresponding approximate distribution within the generalized Pareto family. The choice of the threshold value is a balance between bias and variance. Too low a threshold leads to bias as it will violate the asymptotic basis of the model. However, too high a threshold will lead to a high variance due to too few points to estimate the model with. The standard practice is to adopt as low a threshold as possible, as long as the model still provides a reasonable approximation (Coles, 2001).

Coles (2001) suggests that a method for selecting the threshold is to calculate ψ for a series of thresholds. For thresholds that do not cause high variance, the value of ψ should be constant. A mean residual life plot, a plot of mean excess versus threshold value, is used to select a threshold that does not cause too much bias, shown by a flat line in the plot. The mean excess is calculated by

$$E(Y) = \frac{\sigma}{1 - \psi}, \tag{3}$$

where Y is a distribution that has a GPD. Mean residual life plots can be difficult to interpret, and therefore the selection of a threshold is subjective, however the method provides a framework for selecting a suitable threshold. In this paper, the threshold was kept constant for all seasons, resolutions and climates, therefore a threshold that was valid for all of the analyses was chosen. For the precipitation field, a threshold of 2.5 $\mathrm{mm\,h^{-1}}$ was found to have a low variance and not cause too much bias (e.g. Fig. 1, DJF). A threshold of 45 $\mathrm{m\,s^{-1}}$ was chosen for the wind field. To examine further the nature of the storms resulting in extremes, the track densities are computed for extreme storms using the same thresholds as used in the EVT. The densities are computed using the Kernel method (Hodges, 1996) and storms selected if they attain their maximum in wind speed or precipitation north of 30°N for the T319 simulation.

3. Results

The results for the effect of an increase in resolution, and the effect of a warmer climate, on the intensity distributions of cyclones are discussed later, first for the dynamical fields, then with a particular focus on precipitation. Several different dynamical measures of the intensity of a storm were chosen, 850-hPa maximum winds, 850-hPa maximum vorticity and minimum

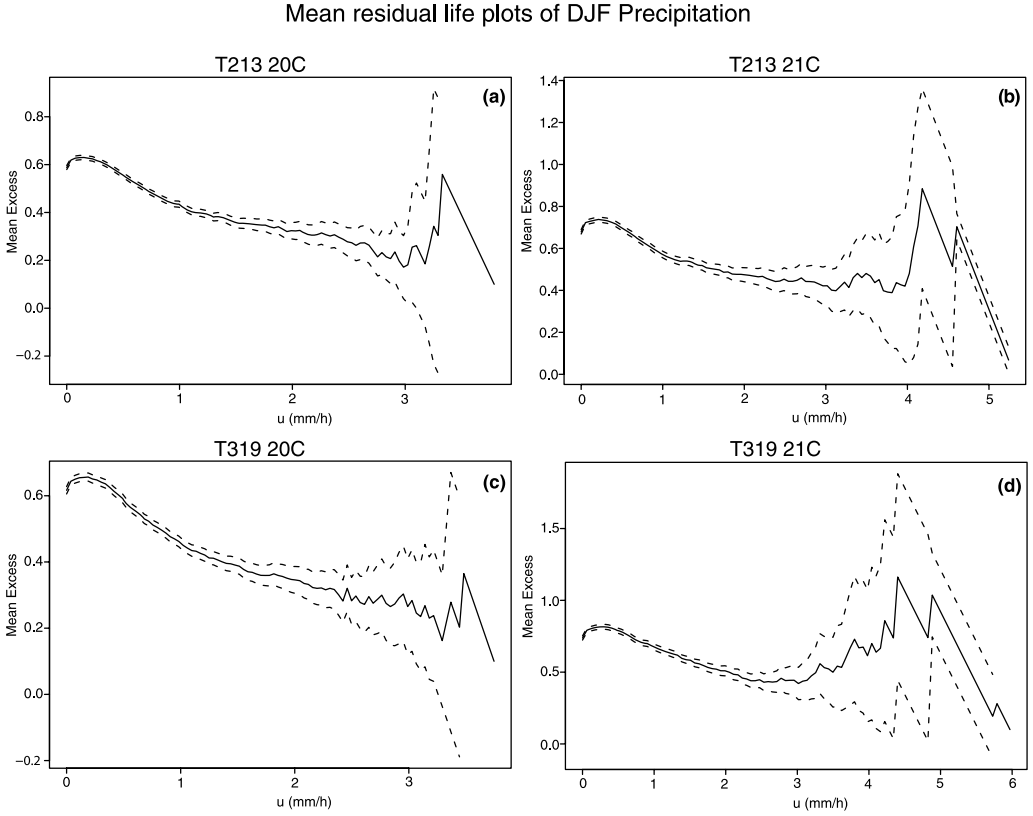

Fig. 1. Mean residual life plots for the DJF precipitation field for a range of threshold values. The range of thresholds where the line is linear indicates the range at which the thresholds do not cause bias. The dashed lines represent the 95% confidence intervals.

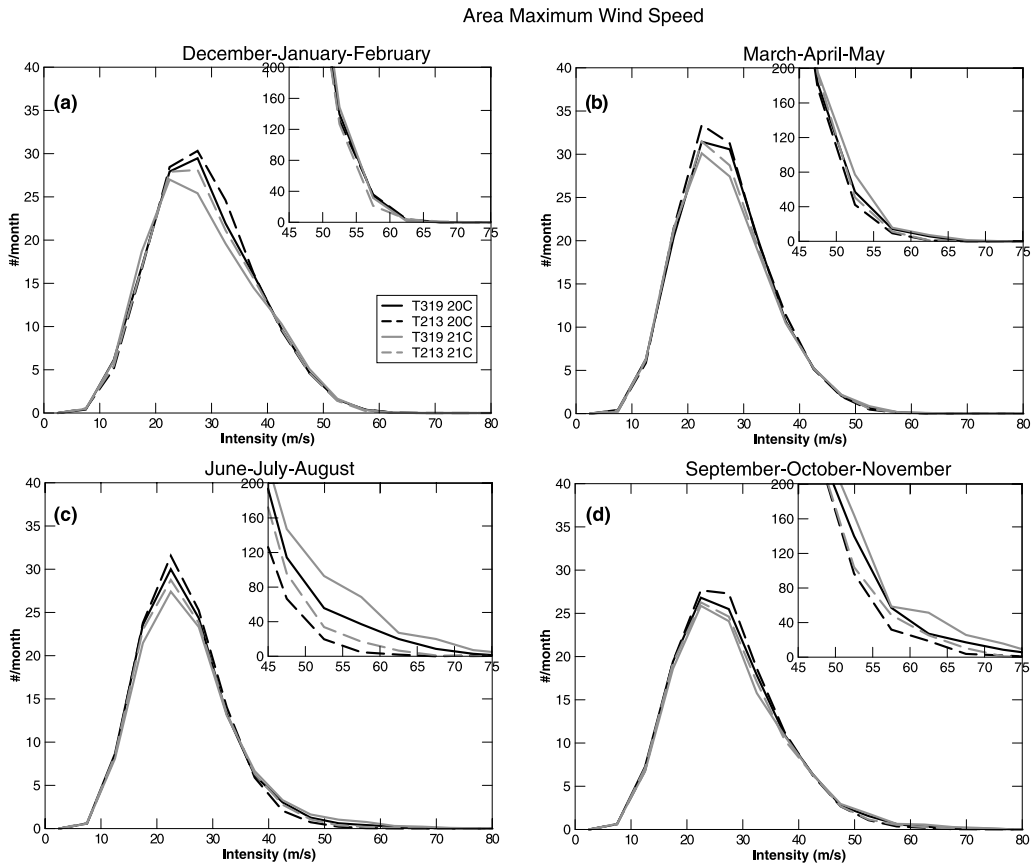

Fig. 2. Maximum 850-hPa wind speed along the storm track within a 5° area of the storm's centre for: (a) DJF, (b) MAM, (c) JJA and (d) SON. The T319 resolution is shown by the solid lines, dashed lines are the T213 resolution. The black lines are for 20C and the grey lines are for 21C. The insets are the tails of the distributions scaled to 30 yr (90 months).

700-hPa area averaged vertical velocity. The MSLP field was investigated but was not very interesting and the results are not shown.

3.1. Winds, Vorticity and Vertical Velocity

The frequency distribution of the full resolution maximum 850-hPa wind intensity along the identified cyclone tracks for the NH for all four seasons: December–January–February (DJF), March–April–May (MAM), June–July–August (JJA) and September–October–November (SON), are shown in Fig. 2. The insets are the tails of the distributions scaled to 30 yr (90 months). The effect of the search radius on the wind field was investigated by Catto (2009), where it was shown that for storms with the strongest winds, these winds almost always occur within 5° of the system centre.

Comparing the T213 resolution (dashed lines) with the T319 resolution (solid lines) in Fig. 2 shows that the effect of an increase in resolution depends on the season. DJF and MAM both show very small changes to the distributions. A slight reduction in the modal intensity is seen, however almost no change is seen in events with intensities >45 m s^{-1}. For JJA and SON, similar magnitudes in the response for the modal intensity are seen, however larger changes are seen in the tails, with a doubling in the number of events with intensities >45 m s^{-1}. This is possibly associated with tropical cyclones (see later) that migrate into the mid-latitudes which can be very sensitive to model resolution (Bengtsson et al., 2007).

The KS test applied to the different resolutions (Table 1) suggest that for the 20C the JJA distributions are statistically different, however for the other 20C distributions it is not possible to reject the null hypothesis at the 95% level. For 21C, the KS test suggests that only MAM does not show statistically different distributions with resolution.

The difference for the extreme events (events with intensities >45 m s^{-1}) is investigated further using the extreme value statistics. A threshold of 45 m s^{-1} was found to ensure a suitable number of extreme events, that is, not creating a high variance, while ensuring that the resulting distribution fits the Generalized Pareto family of distributions, that is, do not create a large bias. Return levels of the GPD analysis for DJF and JJA are shown in Fig. 3.

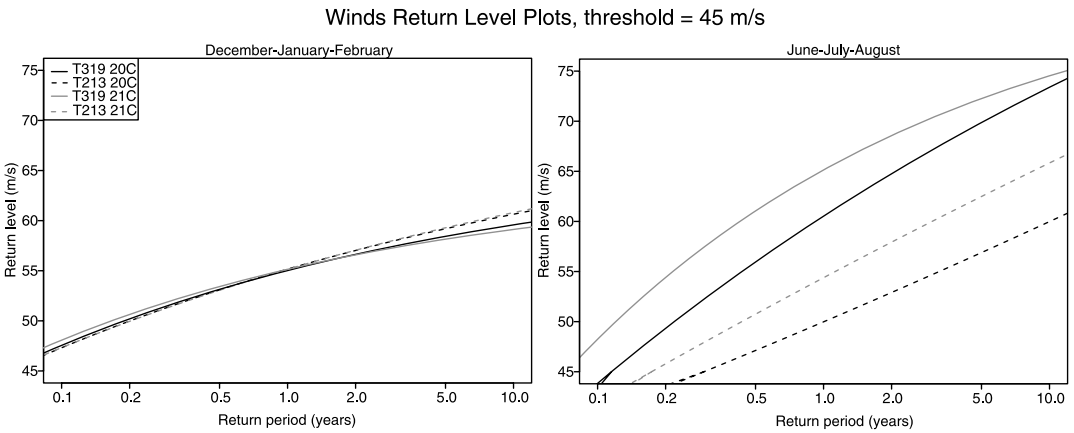

Fig. 3. Return Level Plots for the maximum 850-hPa wind speed along the storm track within a 5° area of the storm's centre for: DJF (left) and JJA (right). The dashed lines represent the T213 resolution and the solid lines represent the T319 resolution. The black lines are for 20C and the grey lines are for 21C.

The effect of the increase in resolution (dashed/solid) is shown to change the return period for JJA, with return periods becoming shorter for a given return level. In the T213 resolution run, an event with a return period of 5 yr has a return level of 55 m s^{-1}. The return period for this return level in the T319 run, again for 20C, is 0.5 yr, that is, a 1 in 5 yr event becomes a 1 in 0.5 yr event due to the increase in resolution. Similar results are seen when comparing the resolutions for 21C. No change in the return periods can be seen for DJF for either climate, which corresponds to what was seen in the tails of the intensity distributions (Fig. 2). The return level plots (Fig. 3) show that DJF for the T319 resolution run, almost no change in the return periods/levels is seen. However, in contrast, JJA shows that a 1 in 5 yr event will become a 1 in 2 yr event.

The effect of a warmer climate can be investigated by comparing the 20C (black) to the 21C (grey) lines in Fig. 2. DJF and MAM show a small decrease in the number of events identified at the modal intensity, and almost no change in the number of events identified with intensities >45 m s^{-1}. JJA and SON again show much larger responses to the effect of a warming climate for events with intensities >45 m s^{-1}, although a similar magnitude of response for the modal intensity. JJA shows the largest response to the warming climate, with 50% more extreme events identified in the warmer climate, for both resolutions.

The KS tests for the effect of a warmer climate on the 850-hPa wind distributions (Table 2) were performed for both the T213 and the T319 integrations. The T213 integration was run for 30 yr whereas the T319 integration was run for 20 yr. This is not taken into account in the KS tests, therefore it can be expected that more robust changes may be seen in the longer T213 integration than the shorter T319 integration, although this was tested and no differences as to whether a particular change can be rejected or not, was observed. The KS tests for DJF and JJA show that the effect of a warmer climate produces statistically different distributions. However, the effect on the SON and MAM distributions shows that the null hypothesis cannot be rejected.

The nature of the storms associated with the extreme winds is further explored by computing the track densities for these storms. The track densities show the spatial distribution of the storms associated with the extreme events used in the extreme value statistics (Fig. 4). It is immediately clear that there are a greater number of storms in DJF than in JJA for both climates, which is also seen in the tails of the intensity distributions (Fig. 2). This is not too surprising as DJF is the period when baroclinic processes dominate and windstorms are more prevalent. However, it can also be seen that there is very little change in the density plots for DJF between the two climates, which is also seen in the return level plots (Fig. 3). However, there is some indication of an increase in the extremes extending into northern Europe in agreement with previous studies (Bengtsson et al., 2006; Pinto et al., 2007). An increase in density is seen for JJA, over both the Pacific and the Atlantic in the warmer climate. From the densities, it is clear that some of these storms have tropical origins, the increase in number reflects the increase in intense tropical cyclones in a warmer climate (Bengtsson et al., 2007).

The increase in resolution is expected to have a larger effect on the maximum 850-hPa relative vorticity (Fig. 5) than winds, as it is a second-order field in terms of derivatives. This is seen by the number of events identified at the modal intensity decreasing by between 15% and 30% with the increase in resolution. This decrease is largest for DJF (Fig. 5a) and smallest for SON (Fig. 5d). There is also a shift in the distributions toward more extreme events in the higher resolution, with events of up to 80 × 10^{-5} s^{-1} seen in the lower resolution T213 run, however events greater than 100 × 10^{-5} s^{-1} are seen in the T319 run. All the distributions in the higher resolution run are also shown to be statistically different from the lower resolution runs (Table 1).

Table 2. Results of the Kolmogorov–Smirnov two-sample test, evaluating whether a warmer climate leads to a statistically significant change in the distributions, for every field and resolution

Variable	Resolution		DJF	JJA	SON	MAM
Winds	T213	D	0.0199	0.0238	0.0104	0.0119
		p	**0.0138**	**0.0049**	0.567	0.3475
	T319	D	0.0252	0.0342	0.0176	0.0152
		p	**0.0126**	**0.0006**	0.1999	0.3117
Vorticity	T213	D	0.0232	0.0577	0.0268	0.0216
		p	**0.0067**	**0.0000**	**0.0011**	**0.0099**
	T319	D	0.0205	0.0841	0.0347	0.0282
		p	0.0713	**0.0000**	**0.0003**	**0.0036**
Vertical velocity	T213	D	0.0256	0.0284	0.0394	0.0235
		p	**0.0006**	**0.0005**	**0.0000**	**0.0027**
	T319	D	0.0216	0.0219	0.0155	0.0191
		p	**0.0494**	0.0845	0.3685	0.1268
Precipitation	T213	D	0.0582	0.07949	0.0632	0.0597
		p	**0.0000**	**0.0000**	**0.0000**	**0.0000**
	T319	D	0.0762	0.00655	0.0631	0.048
		p	**0.0000**	**0.0000**	**0.0000**	**0.0000**

Notes: A *p*-value of less than 0.05 (95%) is chosen as the level at which the null hypothesis should be rejected, being marked in bold. Any value that was $<1 \times 10^{-4}$ is shown to have a value of 0.0000.

The differences in the vorticity distributions are so large that the KS test is redundant.

The response to a warming climate (Fig. 5) is seen to be more dependent on the season. DJF (Fig. 5a) shows almost no change in the distribution due to a warming climate. MAM and SON (Figs. 5b and d) show a small response, with a reduction in the number of events identified at the modal intensity and a slight increase in the number of extreme events. JJA (Fig. 5c) has the largest response, with a reduction in the number of events at the modal intensity and an increase in the number of extreme events, as seen in the wind results. These differences are shown to be statistically significant (Table 2) except for the 21C DJF.

The 700-hPa vertical velocity field (Fig. 6) was investigated as precipitation is associated with strong vertical ascent. The increase in resolution results in large changes to the vertical velocity distributions (Fig. 6) as vertical velocity is highly dependent on horizontal resolution due to the small horizontal scale that it operates on. This can be seen across all the seasons with half the number of events identified at the modal intensity in the T319 run compared to the T213 run. There is also a shift in the distribution toward more negative (ascent) velocities. All the seasons also show the distributions extending to velocities below -1 Pa s^{-1}, less than the -0.5 Pa s^{-1} seen in the T213 resolution. The KS tests (Table 1) show that these differences are due to the increase in resolution, rather than random deviations. As with vorticity, the KS test is redundant for the resolution change as the distributions are so different. Very little change to the distributions due to a warmer climate (Fig. 6) are seen. The changes to the T213 distributions are statistically significant (Table 2), however, at the T319 resolution only the DJF distributions are significantly different. However, there is very little change in the extremes.

3.2. Precipitation

In this section, the effect of resolution and a warmer climate on the precipitation associated with the cyclones is explored. First, however, a sensitivity study was conducted on the trajectories of the storm and the sampling region for measuring the precipitation intensities. The effect of the displacement filter on the maximum intensity distributions of the precipitation field was investigated by removing the filter, but keeping the 2-d duration filter. By excluding the distance criteria, there was around a 60% increase in the number of low-intensity (<0.75 mm h^{-1}) storms identified. The distance criteria had no effect on the distribution of the extreme events (>2.5 mm h^{-1}) identified. Similar results were also seen for both the wind and vorticity fields. Given this paper is looking at the extremes, the distance filter was kept to allow a comparison to the results from Bengtsson et al. (2009), however for more regional studies where intensities are lower this may need to be revised.

The sensitivity study for the size of the spherical cap over which the precipitation is averaged considered a 2.5° and 10° cap as well as the original 5° cap. As the size of the cap is increased, fewer events with intensities >2.5 mm h^{-1} are identified with an increase in the number of low-intensity events. This is due to the increased area for the averaging encompassing larger regions with little or no precipitation. The opposite is true as the size of

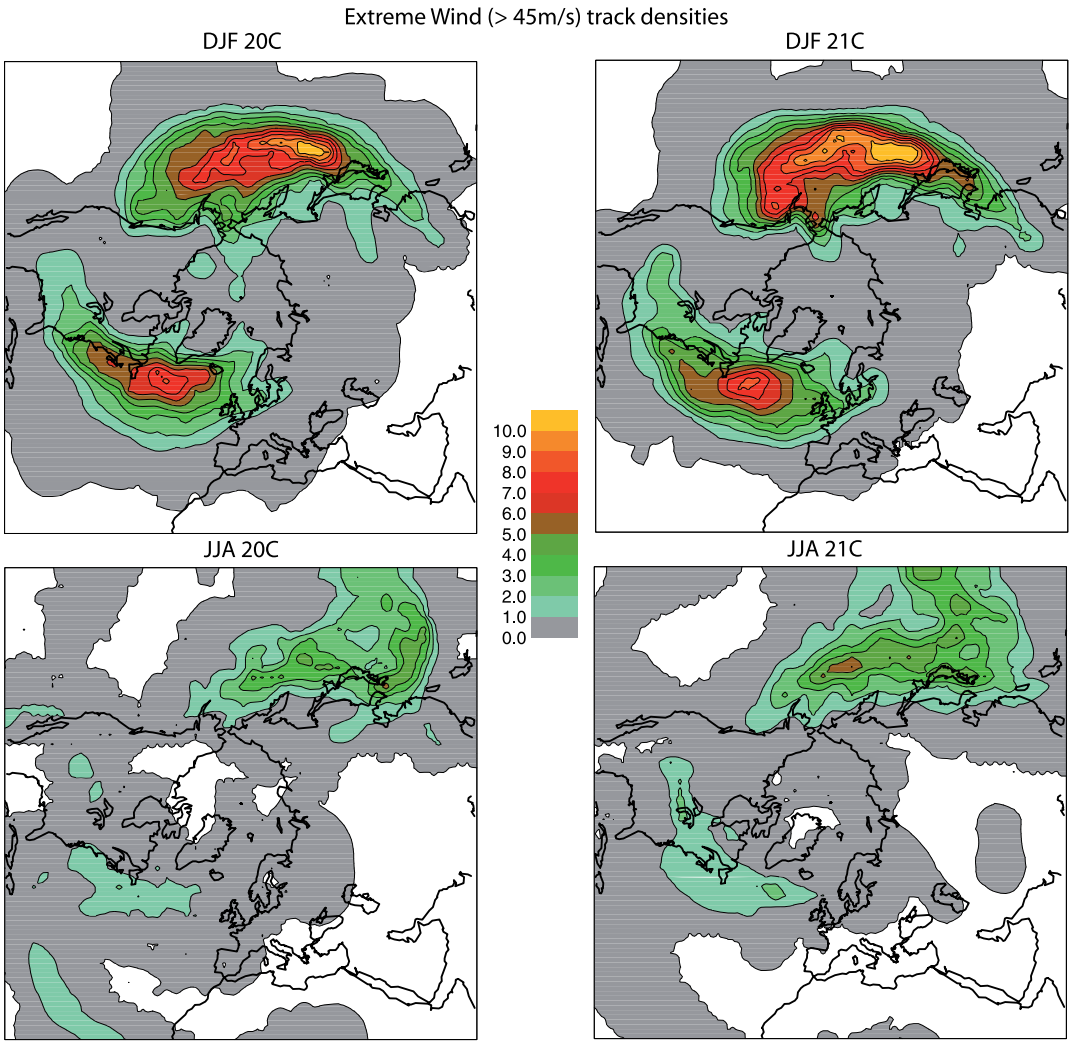

Fig. 4. Track density plots for DJF and JJA wind cyclones with a maximum intensity >45 m s^{-1} within the extratropics. Track density units are number density per month per unit area where the unit area is equivalent to a 5° spherical cap (10^6 km^2).

the cap is reduced, with an increase in the number of extreme events being identified (Fig. 7). The effect on the return periods is to decrease the return period for a given intensity as the size of the cap is decreased, corresponding to the increase in the number of extreme events. For a 10° cap, there were too few events identified for return plots to be generated for the chosen threshold. The cap size was kept at 5° to allow comparison with the results from Bengtsson et al. (2009).

For the full resolution area average precipitation, Fig. 8 shows that events for intensities <1 mm h^{-1}, the increase in resolution results in a decrease in the number of events identified. This decrease is true for events of up to 1.5 mm h^{-1} in SON, which shows the largest magnitude response to the increase in resolution at these intensities. The other seasons all show a similar magnitude of response to each other. The tails of the distributions with intensities >2.5 mm h^{-1}, hereafter referred to as extreme show that the increase in resolution results in an increase in the number of extreme events identified, with upwards of four times the number of events identified in the JJA 20C. An exception to this is DJF 20C, which shows no change in the distribution of the extreme events due to an increase in resolution. This response to resolution between the different climates is not seen in any of the other variables discussed (Section 3.1). It might be expected that a similar result due to the increase in resolution would be seen in the vertical velocity (Fig. 6a), however this does not appear to be the case. The KS tests indicate that an increase in resolution leads to significant differences in the precipitation distributions in all cases, including DJF 20C, except for MAM 21C (Table 1).

Extreme precipitation events are investigated further using extreme value statistics, with the return levels for DJF and JJA using a GPD and a threshold of 2.5 mm h^{-1} shown in Fig. 9. The DJF 20C shows almost no change in the return levels due to an increase in resolution (Fig. 8a). A much larger response is seen for DJF 21C and for both climates in JJA, with the largest

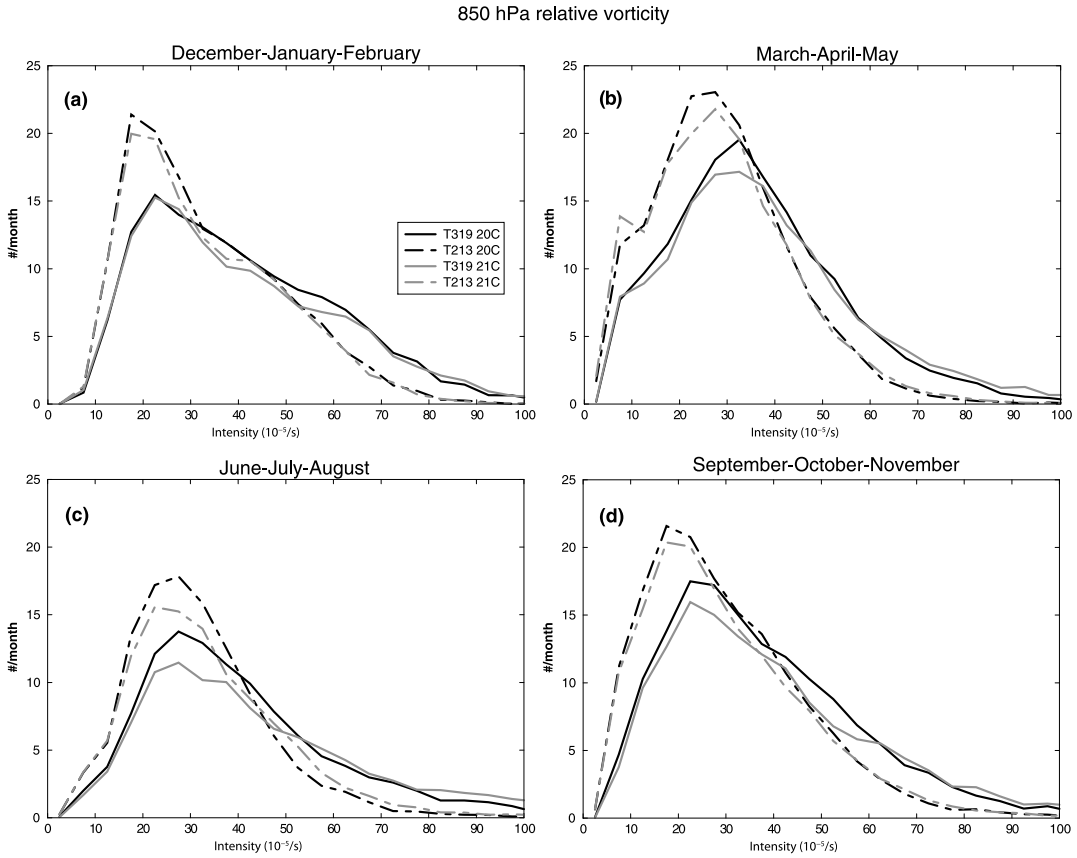

Fig. 5. Maximum vorticity intensity along the storm track within a 5° area of the storm's centre for: (a) DJF, (b) MAM, (c) JJA and (d) SON. The T319 resolution is shown by the solid lines, dashed lines are the T213 resolution. The black lines are for 20C and the grey lines are for 21C.

response seen in JJA 20C where a 1 in 5 yr event becomes a 1 in 0.5 yr event. These increases in the intensity of extreme precipitation events are expected with an increase in resolution as precipitation is a small-scale field. The larger changes during JJA are likely associated with the sensitivity of convective processes to resolution and in particular for tropical cyclones (see later).

The effect of a warmer climate on the precipitation can be seen in both the frequency distributions (Fig. 8) and the return levels (Fig. 9). For events with intensities <1 mm h^{-1}, a decrease in the number of events identified is seen. The extreme events show an increase in the number of events identified, with over four times the number of events identified in the warmer climate. The return level plots show that a 1 in 5 yr event becomes a 1 in 0.5 yr event for DJF. For JJA, an event with a 1 in 5 yr return period decreases to a 1 in a yr event. This response is similar for both resolutions. These results suggest that extreme precipitation events from extratropical storms will become more intense and more frequent. These differences in the distributions due to a warming climate are statistically significant (Table 2).

To examine the nature of the storms leading to extreme precipitation, the track densities are calculated using all the extreme storms (storms with intensities >2.5 mm h^{-1}) that have their maximum north of 30°N. The track densities for the extreme events are shown in Fig. 10. A large change is seen for both DJF and JJA due to a warmer climate, with a significant increase in the density of the tracks in the warmer climate, which agrees with the tails of the intensity distributions (Fig. 8) and the return level plots (Fig. 9). For DJF, this increase is seen in both the Pacific and the Atlantic, although a larger change is seen in the west of the Atlantic, associated with the Colorado cyclogenesis. The effect of a warmer climate on the JJA tracks is seen predominantly in the Pacific, with significant increases due to a warmer climate, although increases over the Atlantic are also seen. The difference in the track densities between the two regions (also seen for the winds) suggests that using a fixed threshold for extreme events may not be suitable when comparing extreme events from different regions. Using a fixed threshold, a much larger number of events is identified in the Pacific than in the Atlantic, which will have an effect on the return level plots. There is some indication that some of these systems are tropical in origin in both the Pacific and Atlantic and the increase in extremes is associated with the intensification of tropical cyclones in a warmer climate seen in other studies, e.g. Bengtsson et al. (2007).

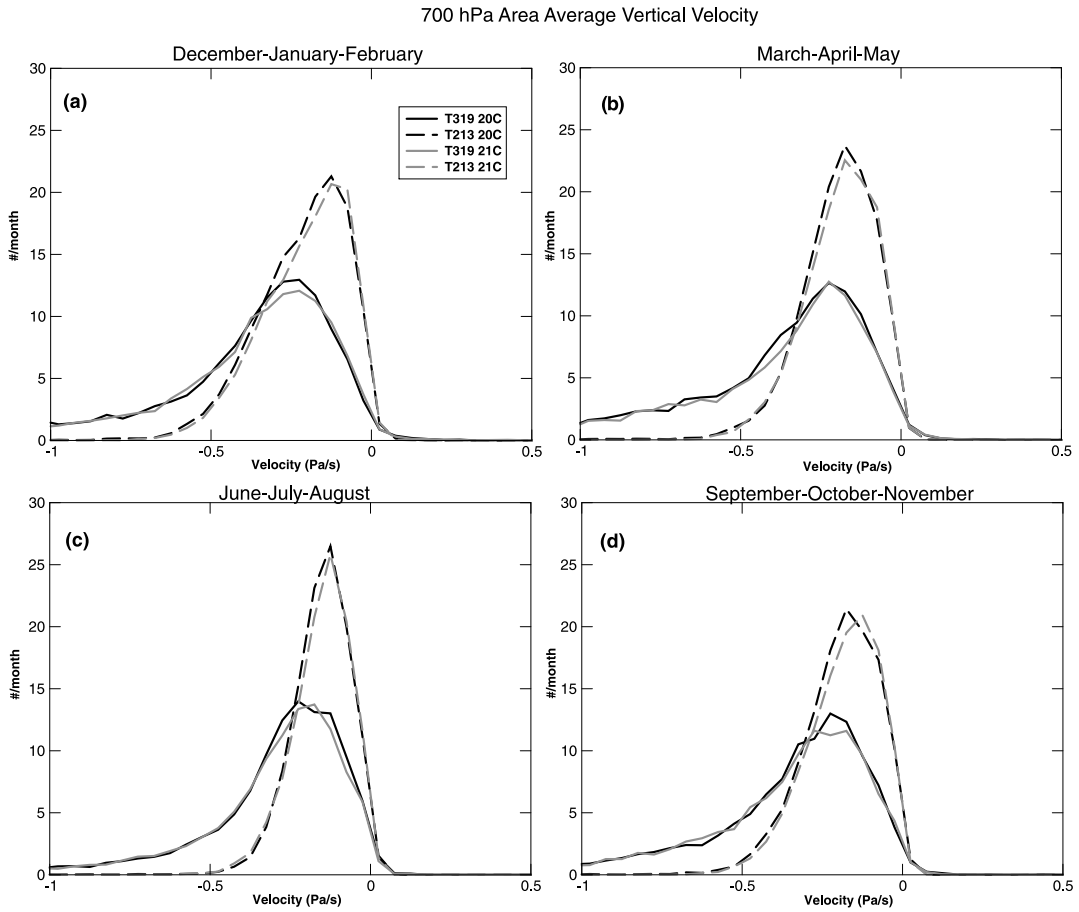

Fig. 6. Area average vertical velocity at 700-hPa along the storm track within a 5° area of the storm's centre for: (a) DJF, (b) MAM, (c) JJA and (d) SON. The T319 resolution is shown by the solid lines, dashed lines are the T213 resolution. The black lines are for 20C and the grey lines are for 21C.

4. Discussion and Conclusions

Extratropical storms have been studied using data from the T319 integration of the atmosphere only ECHAM5 model forced with SST data from a coupled model at lower resolution. The simulation was run for two 20-yr periods representative of the 20th century (1980–2000) and 21st century under the A1B scenario (2080–2100). The properties of these storms have been investigated and compared to the results from T213 simulation of the same model, as used by Bengtsson et al. (2009), which was run for two 30-yr periods representative of the same climates. The study has focused on the effect of an increase in resolution on the dynamical properties of the storms and in particular the precipitation associated with extratropical storms in the NH, as well as looking at the effect of a warmer climate on these events.

Results show that the cyclone properties are highly dependent on resolution, even at these relatively high resolutions for climate models. In fact the resolutions used here are comparable to the resolutions often used in RCM. This raises the important question of what resolutions do we actually need to use to capture cyclone properties, in particular precipitation and to have confidence in their use to predict the future climate. The results also show that the response of the cyclone properties to a warmer climate are also dependent on the model resolution but for either resolution the changes between 20C and 21C are considerably smaller than the changes associated with the change in resolution. The total number of storms identified in the higher resolution run was very similar to the number of events identified in the lower resolution run. The effect of the increased resolution depended on the field investigated. Fields such as the wind speed, a first-order field in terms of derivatives, show a small change due to resolution. Vorticity, a second-order field, and the vertical velocity showed an increase in the number of extreme events, with a corresponding decrease in the number of low-intensity events, typical of a shift in the distribution. The precipitation field showed a large increase in the number of extreme events due to the increase in resolution, except for DJF 20C where no increase was seen. This is likely a consequence of the relative importance of convective processes that are resolution-dependent and are less important during winter.

Similar results as in Bengtsson et al. (2009) for changes due to a warmer climate were found. There is a small change in the

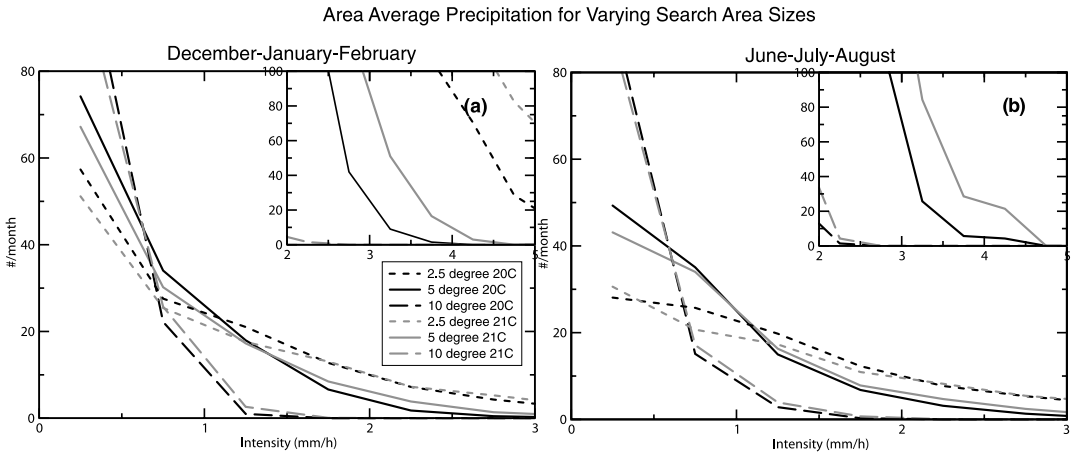

Fig. 7. Sensitivity of the distributions of the precipitation field to the size of the search area from the storm's centre along the storm track for: (a) DJF and (b) JJA. The 2.5° area is shown by the dotted lines, the 5° area is shown by the solid lines and the 10° area is shown by the dashed lines. The black lines are for 20C and the grey lines are for 21C. The insets are the tails of the distributions scaled to 30 yr (90 months).

intensity distributions for wind, with negligible changes to the extremes, except for JJA, which shows a large increase in the number of extreme events. This is thought to be due to an increase in the intensity of tropical cyclones in a warmer climate as discussed in Bengtsson et al. (2007) and which migrate into high latitudes, evidence for this is seen in the track densities. The relative vorticity shows little change in the distributions, again except for JJA, where a shift toward extreme events similar to the results

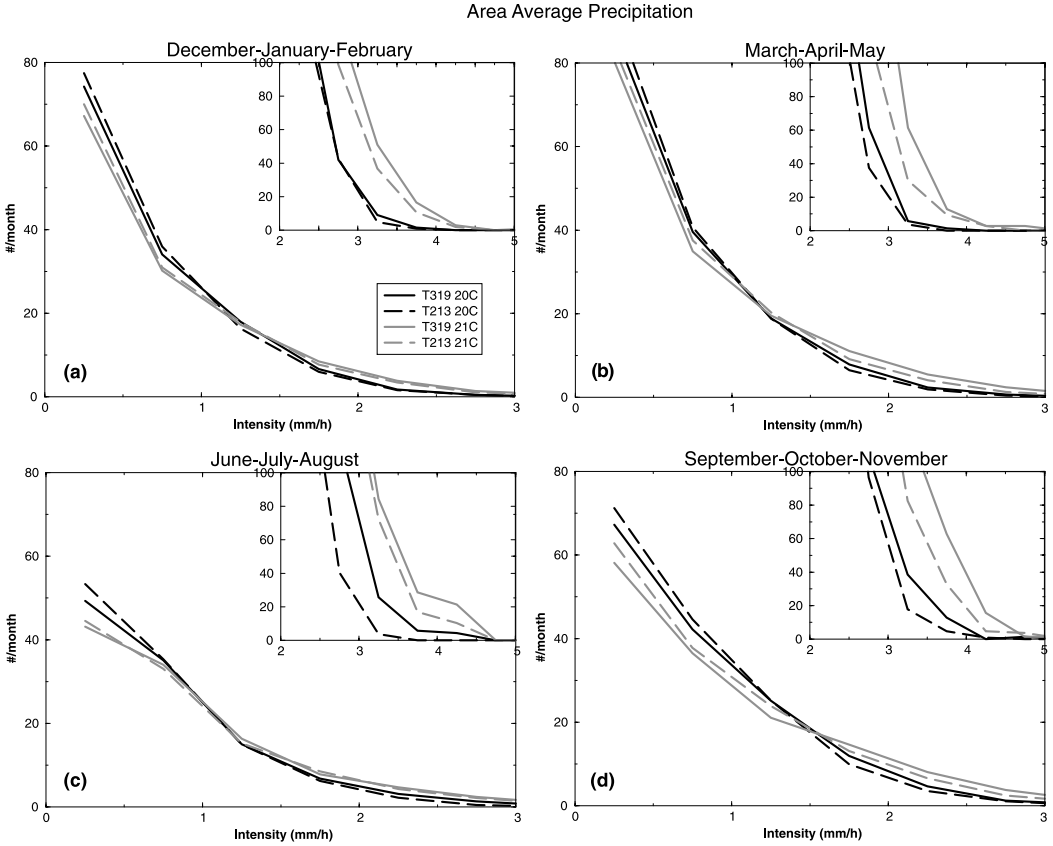

Fig. 8. Area average precipitation along the storm track within a 5° area of the storm's centre for: (a) DJF, (b) MAM, (c) JJA and (d) SON. The T319 resolution is shown by the solid lines, dashed lines are the T213 resolution. The black lines are for 20C and the grey lines are for 21C. The insets are the tails of the distributions scaled to 30 yr (90 months).

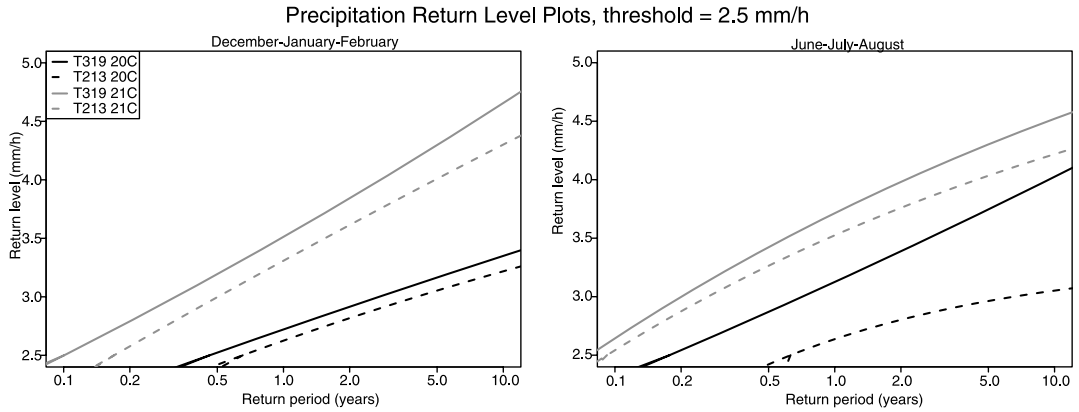

Fig. 9. Return Level Plots for the area average precipitation along the storm track within a 5° area of the storm's centre for: DJF (left) and JJA (right). The dashed lines represent the T213 resolution, the solid lines represent the T319 resolution. The black lines are for 20C and the grey lines are for 21C.

for wind. Again this is likely related to tropical systems migrating into the mid-latitudes. The changes to the vertical velocity distributions are also negligible. However, large changes in the precipitation distributions are seen, with significant increases in the number of extreme events identified in the warmer climate. The return period for a summer 1 in 5 yr event has been shown to become a 1 in a yr event. A similar reduction in the return period is seen for winter events. Previous, non-precipitation associated, POT GPD work on the T63 integration of the ECHAM5 model by Della-Marta and Pinto (2009) and Sienz et al. (2010) also showed, at a more regional scale, that the return periods for the maximum vorticity of winter (October–March) storms, for all intensities, decrease due to a warmer climate, with a particular focus on the British Isles, North Sea and western Europe, however, this is more likely related to a shift in the storm tracks. The magnitude of the changes due to a warmer climate in the T319 integration is similar to the magnitude of the changes seen in the T213 integration, apart from the DJF 20C precipitation exception.

The results in this paper have been compared to earlier results by Bengtsson et al. (2009), but not to any validation data, such as ERA-40 or ERA-Interim. This type of validation is difficult for precipitation due to spin-up in the reanalyses. Bengtsson et al. (2009) discuss the ability of the T213 integration of the model used in this study to reproduce the typical lifecycle and structure of storms when compared with ERA40. Ulbrich et al. (2008) also suggest that the ECHAM5 model provides realistic results. The role of internal variability is not discussed due to the requirement for much longer simulations at these resolutions. CMIP5 may offer some scope for this although the CMIP5 models will mostly be at much lower resolutions than used here. The T319 integration results suggest that with an increase in the resolution, more extreme events are identified in both climates specifically in terms of precipitation. This study suggests that events such as the summer 2007 floods and the November 2009 flood experienced in the United Kingdom could become more severe, due to the increase in the intensity of the extreme precipitation events, although a more regional-based analysis of the data is required to confirm this. This agrees with the RCM projections by Nikulin et al. (2011) for central Europe. This has large implications for managing these events, with the potential for more people to be affected by floods.

The increase in JJA precipitation and winds in a warmer climate could be due to tropical cyclones as discussed by Bengtsson et al. (2007). There is no apparent increase in dynamical variables such as winds, vorticity or vertical velocity in DJF, when storms are at their most intense, even though an increase in precipitation is seen, for the whole NH. This was also found in other studies, for example, Bengtsson et al. (2009) and Watterson (2006). Bengtsson et al. (2009) suggest that a possible reason is due to the competing processes between a decrease in low-level baroclinicity, associated with weaker temperature gradients, against an increase in latent heat from the increase in precipitation. The study of O'Gorman (2010) suggests that the increase latent heat affects smaller scale convective storms more in JJA. This is reflected to some extent in the results here where storms are more intense in precipitation in JJA. Other studies, for example, Pinto et al. (2007, 2009), have shown an increase in the upper air baroclinicity, as well as an increase in the polar jet intensity, specifically for the North Pacific basin. Dacre and Gray (2009) also suggest an increase in high-latitude cyclones that are formed when a large upper level trough moves over the ocean (Deveson et al., 2002), due to a warmer climate. A better understanding of the diabatic processes that occur in storms is needed to better inform whether the increase in precipitation will lead to such consequences. It is also noted that the T319 integration was only run for two 20-yr periods, which is quite short. To further test the robustness of the results, it would be useful to have much longer runs for each climate. Even the 30-yr periods of the T213 simulation can be considered rather short for robust statistics. In fact this is the main reason for concentrating on hemispheric statistics rather than regional statistics since

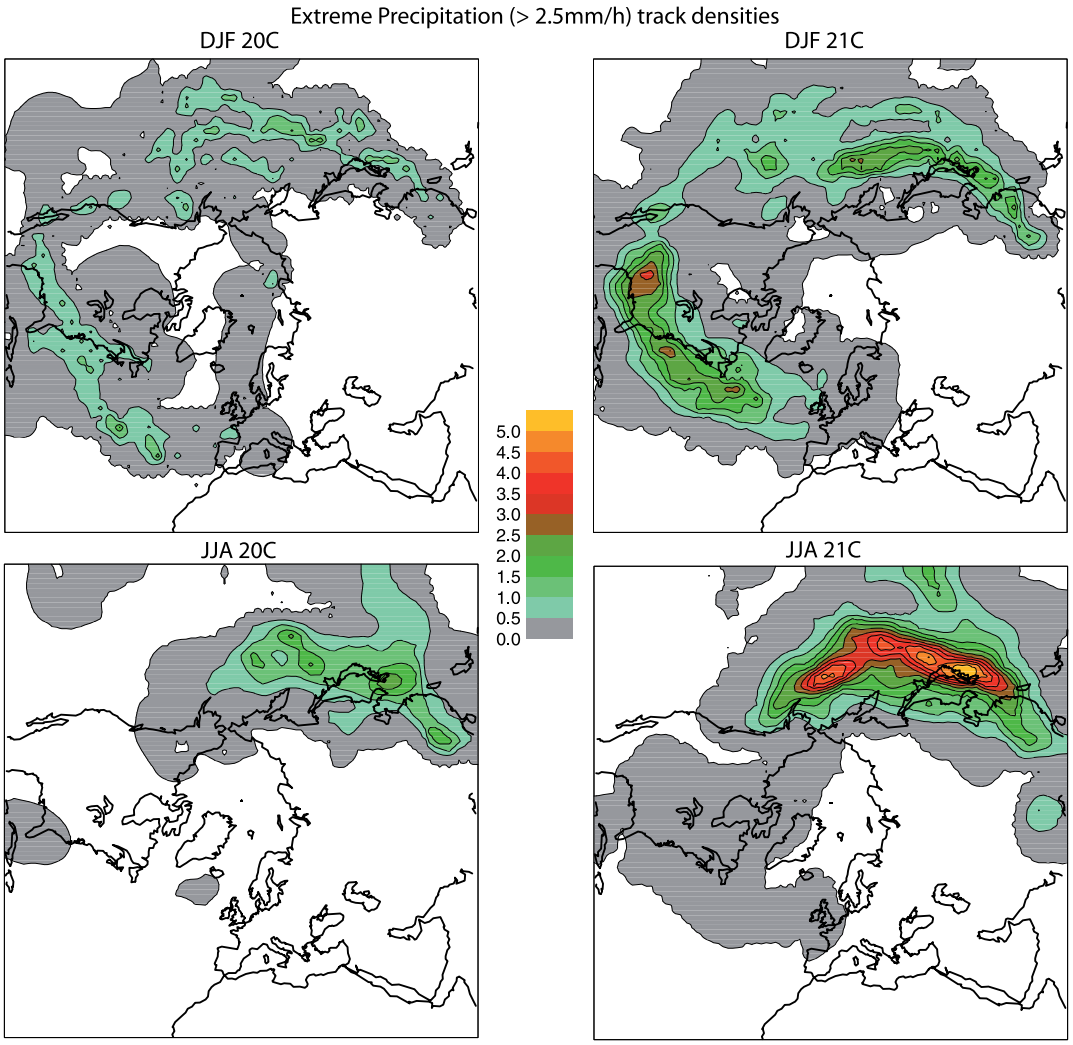

Fig. 10. Track density plots for the DJF and JJA area averaged precipitation cyclones with a maximum intensity >2.5 mm h^{-1} within the extratropics. Track density units are number density per month per unit area where the unit area is equivalent to a 5° spherical cap (10^6 km^2).

for regions such short time periods will introduce even larger sampling uncertainties.

A more regional analysis may show different results due to changes in the storm track location, or more local effects. However, as noted earlier, if comparing different regions using extreme value statistics, it is important to consider the threshold used, and whether a fixed threshold across all the regions is suitable, or varying the thresholds may be more appropriate. The horizontal resolution of the T319 integration of the ECHAM5 model used in this study is about 40 km, which is a similar resolution to some RCMs. To investigate the effect of a warmer climate on precipitation for more specific areas, for example the United Kingdom, extreme events could be downscaled to a very high resolution of 1–4km to better examine cyclone properties, in particular precipitation. However, this requires the computing resources and as with other studies, the results will depend on the driving model. A more attractive solution is to use GCM at very high resolutions (∼10 km or less) which is now beginning to happen in projects such as ATHENA (Jung et al., 2011) though significant resources are required.

5. Acknowledgments

The authors would like to thank the two reviewers for their comments on the paper.

References

Bengtsson, L., Hodges, K. I. and Roeckner, E. 2006. Storm tracks and climate change. *J. Clim.* **19**, 3518–3543.

Bengtsson, L., Hodges, K. I., Esch, M., Keenlyside, N., Kornbleuh, L. and co-authors. 2007. How may tropical cyclones change in a warmer climate? *Tellus* **59A**, 539–561.

Bengtsson, L., Hodges, K. I. and Keenlyside, N. 2009. Will extratropical storms intensify in a warmer climate? *J. Clim.* **22**, 2276–2301.

Blackburn, M., Methven, J. and Roberts, N. 2008. Large-scale context for the UK floods in summer 2007. *Weather* **63**, 280–288.

Catto, J. 2009. *Extratropical Cyclones in HiGEM: climatology, structure and future predictions*, PhD thesis, University of Reading.

Christensen, O. and Christensen, J. 2004. Intensification of extreme European summer precipitation in a warmer climate. *Glob. Planet. Change* **44**, 107–117.

Coles, S. 2001. *An Introduction to Statistical Modeling of Extreme Values*, 3rd edition, Springer, London.

Dacre, H. and Gray, S. 2009. The spatial distribution and evolution characteristics of North Atlantic cyclones. *Mon. Weather Rev.* **137**, 99–115.

Della-Marta, P. and Pinto, J. 2009. Statistical uncertainty of changes in winter storms over the North Atlantic and Europe in an ensemble of transient climate simulations. *Geophys. Res. Lett.* **36**, L14703, doi:10.1029/2009GL038557.

Deveson, A., Browning, K. and Hewson, T. 2002. A classification of FASTEX cyclones using a height-attributable quasi-geostraphic vertical-motion diagnostic. *Q. J. R. Meteorol. Soc.* **128**, 93–117.

Fowler, H., Ekström, M., Blenkinsop, S. and Smith, A. 2007. Estimating change in extreme European precipitation using a multimodel ensemble. *J. Geophys. Res.* **112**, D18104, doi:10.1029/2007JD008619.

Frei, C., Shar, C., Luthi, D. and Davies, H. 1998. Heavy precipitation processes in a warmer climate. *Geophys. Res. Lett.* **25**, 1431–1434.

Froude, L. 2010. TIGGE: comparison of the prediction of northern hemisphere extratropical cyclones by different ensemble prediction systems. *Weather and Forecast.* **25**, 819–836.

Grumm, R. 2010. The historic storm of 24-26 October 2010. Technical Report 2010-10-26, National Weather Service, Pennsylvania State University, USA.

Held, I. and Soden, B. 2006. Robust responses of the hydrological cycle to global warming. *J. Clim.* **19**, 5686–5699.

Hodges, K. 1995. Feature tracking on the unit sphere. *Mon. Weather Rev.* **123**, 3458–3465.

Hodges, K. 1996. Spherical nonparameteric estimators applied to the UGAMP model integration for AMIP. *Mon. Weather Rev.* **124**, 2914–2932.

Hodges, K. 1999. Adaptive constraints for feature tracking. *Mon. Weather Rev.* **127**, 1362–1373.

Hoskins, B. and Hodges, K. 2002. New perspectives on the northern hemisphere winter storms tracks. *J. Atmos. Sci.* **59**, 1041–1061.

Maraun, D., Wetterhall, F., Ireson, A., Chandley, R., Kendon, E. and co-authors. 2010. Precipitation downscaling under climate change: recent developments to bridge the gap between dynamical models and the end user. *Rev. Geophys.* **48**, RG3003, doi:10.1029/2009RG000314.

Nakicenovic, N., Alcamo, J., Davis, G., de Vries, B., Fenhann, J. and co-authors. 2000. Special report on emissions scenarios, Cambridge University Press.

Nikulin, G., Kjellström, E., Hansson, U., Strandberg, G. and Ullerstig, A. 2011. Evaluation and future projections of temperature, precipitation and wind extremes over Europe in an ensemble of regional climate simulations. *Tellus* **63A**, 41–55.

O'Gorman, P. 2010. Understanding the varied response of the extratropical storm tracks to climate change. *Proc. Natl. Acad. Sci. USA* **107**, 19 176–19 180.

Pinto, J., Ulbrich, U., Leckebusch, G., Spangehl, T., Reyers, M. and co-authors. 2007. Changes in storm track and cyclone activity in three SRES ensemble experiments with the ECHAM5/MPI-OM1 GCM. *Clim. Dyn.* **29**, 195–210.

Pinto, J., Zacharias, S., Fink, A., Leckesbusch, G. and Ulbrich, U. 2009. Factors contributing to the development of extreme North Atlantic cyclones and their relationship with the NAO. *Clim. Dyn.* **32**, 711–737.

Pitt, M. 2008. The Pitt Review: learning lessons from the 2007 floods, Technical report, Cabinet Office.

Roeckner, E., Bäuml, G., Bonaventura, L., Brokopf, R., Esch, M. and co-authors. 2003. The atmospheric general circulation model ECHAM5. Part I: model description, Technical Report 349, Max Planck Institute for Meteorology, Hamburg, Germany.

Roeckner, E., Brasseur, G., Giorgetta, M., Jacob, D., Jungclaus, J. and co-authors. 2006. Climate projections for the 21st century, Technical Report 28, Max Planck Institute for Meteorlogy, Hamburg, Germany.

Sibley, A. 2010. Analysis of extreme rainfall and flooding in Cumbria 18–20 November 2009. *Weather* **65**(11), 287–292.

Siegel, S. 1956. *Nonparametric Statistics for the Behavioral Sciences*, International Student edition, McGraw-Hill International Book Company, Auckland, New Zealand.

Sienz, F., Schneidereit, A., Blender, R., Fraedrich, K. and Lunkeit, F. 2010. Extreme value statistics for North Atlantic cyclones. *Tellus* **62A**, 347–360.

Jung, T., Miller, M. J., Palmer, T. N., Towers, P., Wedi, N. and co-authors. 2011. High-resolution global climate simulations with the ECMWF model in project athena: experimental design, model climate and seasonal forecast skill. *J. Clim.* In press.

Ulbrich, U., Brücher, T., Fink, A., Leckebusch, G., Krüger, A. and co-authors. 2003. The central European floods of August 2002: Part 1: rainfall periods and flood development. *Weather* **58**, 371–377.

Ulbrich, U., Pinto, J., Kupfer, H., Leckesbusch, G., Spangehl, T. and co-authors. 2008. Changing northern hemisphere storm track in an ensemble of IPCC climate change simulations. *J. Clim.* **21**, 1669–1679.

Watterson, I. 2006. The intensity of precipitation during extratropical cyclones in global warming simulations: a link to cyclone intensity? *Tellus* **58A**, 82–97.

Wernli, H., Dirren, S., Liniger, M. and Zillig, M. 2002. Dynamical aspects of the life cycle of the winter storm 'lothar'. *Q. J. R. Meteorol. Soc.* **128**, 405–429.